Decoding temporal information through slow lateral excitation in the olfactory system of insects

Thomas Nowotny[1], Mikhail I. Rabinovich[1], Ramon Huerta[1],
and Henry D. I. Abarbanel[1,2]

[1]Institute for Nonlinear Science, University of California San Diego, La Jolla, CA 92093-0402

[2]Department of Physics and Marine Physical Laboratory (Scripps Institution of Oceanography), University of California San Diego, La Jolla, CA 93093-0402

Corresponding Author: Thomas Nowotny

Institute for Nonlinear Science, UCSD

9500 Gilman Dr.

La Jolla, CA 92093-0402

Phone: 858-534-6876

FAX: 858-534-7664

email: tnowotny@ucsd.edu

Keywords: Olfaction, odor representation, temporal coding, sparse coding, mushroom body, Kenyon cells

Abstract

Sensory information is represented in a spatio-temporal code in the antennal lobe, the first processing stage of the olfactory system of insects. We propose a novel mechanism for decoding this information in the next processing stage, the mushroom body. The Kenyon cells in the mushroom body of insects exhibit lateral excitatory connections at their axons. We demonstrate that slow lateral excitation between Kenyon cells allows one to decode sequences of activity in the antennal lobe. We are thus able to clarify the role of the existing connections as well as to demonstrate a novel mechanism for decoding temporal information in neuronal systems. This mechanism complements the variety of existing temporal decoding schemes. It seems that neuronal systems not only have a rich variety of code types but also quite a diversity of algorithms for transforming different codes into each other.

1 Introduction

In recent years a lot of experimental evidence for temporal coding of information has been collected in olfactory [Laurent et al., 1998; Laurent, 1999; Laurent et al., 2001], auditory [Jeffres, 1948; Leibold et al., 2002; Lu et al., 2001], visual [v. Rullen and Thorpe, 2001] and tactile systems [Ahissar et al., 1997; Ahissar et al., 2000], as well as in the hippocampus [Wallenstein et al., 1998; Fortin et al., 2002].

The formation of spatio-temporal coding (sometimes also referred to as identity-temporal or ensemble-temporal coding) in the hippocampus is related to behavioral tasks following a temporal sequence [Fortin et al., 2002]. In the example of the tactile system the sensory information from whiskers is encoded in the identity of active neurons for vertical localization but in a temporal code induced by whisker swiping for horizontal information [Ahissar et al., 1997; Ahissar et al., 2000]. Examples of temporal encoding in the visual system are numerous. We have, for example, temporal patterns found in lateral geniculate nucleus [Reinagel and Reid, 2000], temporal coding of contrast [Reich et al., 2001] and general temporal codes in visual cortex [Reich et al., 2000]. Temporal information processing in the auditory system is mainly used for sound location in a three dimensional environment utilizing very precise spike timings [Jeffres, 1948; Leibold et al., 2002] but there is also evidence for non-trivial processing of the temporal structure of sound stimuli in general [Lu et al., 2001].

In the olfactory system temporally structured activity is generated even if the stimulus has no temporal structure itself [Wehr and Laurent, 1999]. It has been demonstrated that such temporal coding plays a role in enhancing the discrimination of similar odors [Stopfer et al., 1997; Laurent et al., 1998; Teyke and Gelperin, 1999].

Several methods to decode temporal information in neuronal systems have been proposed. The oldest we are aware of [Jeffres, 1948] uses delay lines and coincidence detectors to explain the mechanisms of sound location. In more recent work Buonomano et al. showed that a random network of neurons with excitatory and inhibitory synapses having realistic properties is able to transform temporally differing input into spatially different activation patterns [Buonomano and Merzenich, 1995; Buonomano et al., 1997]. Even more recently, experimental observations of the encoding-decoding process in tactile systems indicate that temporal information in these systems is gated through the thalamus [Ahissar et al., 1997; Ahissar et al., 2000] to yield a spatial rate code.

In this paper, we analyze the role of local excitatory connections for temporal decoding in the olfactory system of insects using the locust as our main model system.

The second information processing stage of the olfactory system of the locust, the antennal lobe (AL), has been subject to a thorough theoretical analysis [Rabinovich et al., 1998; Rabinovich et al., 2001; Bazhenov et al., 2001b; Bazhenov et al., 2001a; Laurent et al., 2001]. In the AL the dynamical interplay of excitatory and inhibitory connections between projection neurons (PNs) and local interneurons (LNs) produces sequences of activity that map uniquely to the encountered odor [Stopfer et al., 2003]. Odor identity as well as its concentration are encoded in these sequences of activity.

The present work focuses on the next stage of neural processing in which the information, encoded in the complex dynamics of the AL, is projected

onto a larger screen, the mushroom body (MB). The Kenyon cells (KC) in the MB seem to be coincidence detectors for synchronized activity in the AL. It has been shown that the resulting code in the MB is sparse [Perez-Orive et al., 2002]. In addition to the direct projection from the AL to the MB there is also a global feed-forward inhibition mediated by lateral horn interneurons (LHIs) that resets the activity of the KCs in the MB every $50\,ms$. This reset mechanism cuts the spatio-temporal code of the AL into snapshots of spatial activity patterns.

Our inquiry rests on a paradox. The KCs have local excitatory axo-axonal connections to their nearest neighbors but to date the function of these connections is unclear especially because the global inhibition stops the propagation of activity every $50ms$. Furthermore, if the connections were strong and fast enough to affect neighboring KCs within one $50ms$ cycle of activity this would lead to a non-sparse code which is not observed.

Our main hypothesis is that if the lateral excitation between KCs is sufficiently slow it can be used to decode temporal information across activity cycles. We show that lateral slow excitation can transform a given sequence of activity in the AL into a spatial representation in the MB that is significantly different from the representation of any permutation of that sequence. This way the temporal information of the order of the sequence of activity snapshots in the MB is conserved. This might otherwise be lost during integration of MB activity in downstream areas.

2 Biological morphology

The olfactory circuits of the locust are known accurately [Perez-Orive et al., 2002]. About 90000 olfactory receptor neurons in each antenna project through $\approx$ 900 glomeruli to the corresponding AL containing $\approx$ 830 projection neurons (PN) and $\approx$ 300 LN. The PNs of each AL contact $\approx$ 600 of a total of $\approx$ 50000 KCs in the ipsilateral MB through the calyx. In return each KC receives input from $\approx 10-20$ PNs. This pathway seems to be the only olfactory input to the MB. There also seems to be no direct feedback from the MB to the AL.

The KC of the MB are subject to a periodic global inhibition due to the activity of LHIs which are excited by input from the PNs of the AL. The activity of the LHIs exhibits an approximate phase shift of $\approx 180^\circ$ with respect to the average activity of the PNs or - more or less equivalently - to the observed local field potential in the calyx.

The KCs project to the α, β and γ-lobes through axons which are densely packed in nerve fibers. It has been known for some time that the axons have chemical connections within these nerve fibers establishing a local hexagonal lattice structure within the otherwise seemingly unconnected KCs [Leitch and Laurent, 1996]. The type of connection has not yet been determined unambiguously but they are suspected to be excitatory. These connections are the essential ingredient for the decoding mechanism suggested in this work.

The output of the AL is the synchronous firing of small groups of PNs. These groups of active PNs evolve in a slow switching pattern. Typically in the order of 200 PNs respond in groups of $\approx$ 30 synchronously firing neurons to each odor [Wehr and Laurent, 1996; Laurent et al., 1996]. Recent experiments indicate even larger group sizes in this activity. This type of dynamical activity has been argued to result from neural circuitry built on the principle of winnerless competition [Rabinovich et al., 2001].

3 Functional principle

Our main hypothesis is that the KCs in the MB form a device that transforms the dense spatio-temporal code generated by the AL into a sparse spatial code. The mechanism we suggest to perform this task only requires a sufficient size of the MB and a local structure of slow excitatory connections. No specific connectivity between the AL and the MB is necessary.

The basic mechanism for the transformation of the spatio-temporal code is illustrated in figure 1. The individual KCs act as coincidence detectors for the synchronous PN input with some given threshold. The coincidence detection responds to the spatial part of the spatio-temporal code. The threshold together with the known connectivity statistics determines the average initial activity of the KCs in response to an odor. If a given KC detects a coincidence of sufficiently many PN inputs, it will fire an isolated spike. This will excite the neighbors of this particular KC through the local excitatory connec-

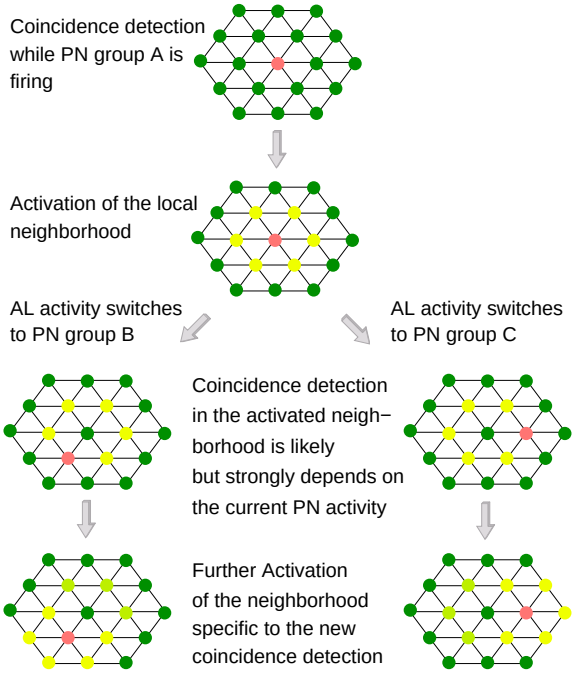

Figure 1: Illustration of the transformation of temporal into spatial information. If a coincidence detection occurs the local excitatory connections activate the neighbors of the active neuron (yellow neurons in the second row). Coincidence detection of input is now more probable in these activated neighborhoods than in other KCs. Which of the neighbors might fire a spike however depends on the activity of the PNs in the next cycle. It might be a different neuron for an active group B of PNs (left side) than for active group C (right side). In this way local sequences of active KC form which depend on the identity of active PNs (coincidence detection) as well as on the temporal order of their activity (activated neighborhoods).

tions. In the temporally next cycle of PN activity these neighbors will be more receptive to input from the AL than in their resting state, i.e., fewer coincident inputs than in the previous cycle will suffice to trigger a spike in these neurons. Depending on the input in the next cycle of PN activity it is therefore likely to have a spike in a KC in the neighborhood of the originally active KC. This will in its turn activate its neighbors and so on. By this mechanism small clusters of active neurons are formed whose size and shape depend on the identity *and* temporal order of the input. It obviously is essential for

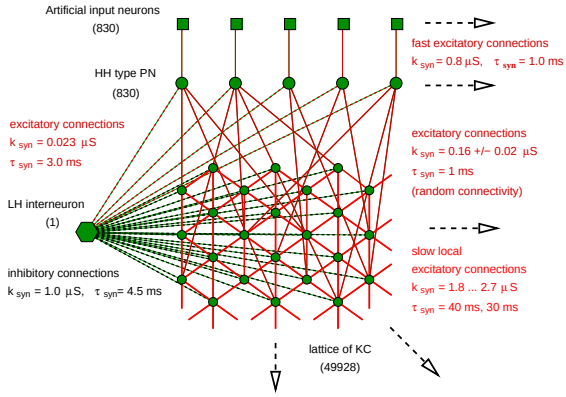

Figure 2: Morphology of the computer model. Excitatory synapses are shown as red lines, inhibitory connections as black lines. Thickness and texture of the lines hint to the strength of the connections.

the functionality that the local excitatory connections are effective longer than one activity cycle of the PN input. Equally important is an adequate connectivity statistics allowing the subsequent coincidence detection in the activated neighborhood KC of active KCs.

4 Numerical Simulation

Because the statistical properties of the connectivity between AL and MB play a crucial role in the suggested function of the KCs the system was simulated in a realistically sized network. We used a set of $158 \times 316 \approx 50,000$ integrate and fire neurons to represent the KCs in the MB. These very simple neurons are adequate for the KCs as they only need to produce a single spike on an infrequent basis. They are connected in a hexagonal lattice by excitatory Rall-type synapses (see Appendix A). The input from the AL stems from 830 Hodgkin-Huxley type model neurons which are induced to spike synchronously in randomly chosen groups of 30 neurons. The active PN neurons spike every $50\,ms$ and the group of active PN neurons is switched every $250\,ms$. The PNs have a fixed probability $p = 600/50000$ to be connected to each KC leading to about 600 connections for each PN.

The feed-forward periodic global inhibition of the LHIs is implemented by one Hodgkin-Huxley type neuron with slow calcium dynamics. It receives input

from all PNs and inhibits all neurons in the KC lattice. The morphology of the computer model is depicted in figure 2. Details of the neuron and synapse models used are given in Appendix A.

Up to this point the simulation is just a crude image of the real system without any specifics about its biological functionality. It is common understanding that the KCs in the MB work as coincidence detectors. We adopted this view and chose the time scale of the PN-KC connections to be $\tau_{\text{syn}} = 1\,ms$; namely, small. This makes the KCs very sensitive to the relative timing of incoming input from the PNs and lets them function as coincidence detectors. The synaptic strength of the PN-KC connections needs to be carefully adjusted to account for the observed initial KC activity in an odor response. It turns out that a constant synaptic strength of these connections cannot account for the activity level observed. We, therefore, introduced an additive Gaussian jitter on the synaptic strengths, in particular for a PN ($i = 1, ..., n_{\text{PN}}$) to KC ($j = 1, 2, ..., n_{\text{KC}}$) connection, we use

$$g_{ij} = \begin{cases} \bar{g} + \delta g & \text{with probability } p \\ 0 & \text{with probability } 1 - p \end{cases} \quad (1)$$

where $\bar{g}$ is the (fixed) average value and δg_{ij} are independent identically distributed (iid) Gaussian random variables with mean 0 and standard deviation σ. For a detailed analysis see Appendix B.

To implement the functional principle described above the local excitatory connections need to be sufficiently slow to still take effect in the next cycle of synchronized PN activity. We therefore tried connections with time scale $\tau_{\text{KC}} = 30\,ms$ and $40\,ms$. The synaptic strength then again needs to be adjusted carefully to be strong enough to allow the temporal decoding described above and to be not to strong to avoid excessive KC activity in form of propagating waves. Appendix B explains the heuristics leading to the values used in the simulation.

5 Results

To test the transformation principle we randomly chose ensembles A, B, C of 30 PN each and activated these ensembles in different temporal orders. The same ensembles A, B, and C were used in all simulations. If the mechanism was implemented successfully the activation of $A \to B \to C$ should lead to a different activation pattern in the KC lattice than $B \to A \to C$ or $A \to C \to B$.

In figure 3 the differences in the average activity of all the KCs for input $A \to B \to C$ compared to input $A \to C \to B$ is shown for local synapses with time constant $\tau_{\text{syn}} = 40\,ms$ and synaptic strength $k_{\text{syn}} = 2.5\,\mu S$. (See the equations for synaptic current in Appendix A.) Clearly, the activity is specific to the order of the presented sequence. Furthermore the difference in activity occurs preferentially at small clusters. The differences of activity between the other two pairings are similar. With stronger local synapses the overall activity and the difference in activity for different input sequences grow. Figure 4 shows an example for $\tau_{\text{syn}} = 40\,ms$ and $k_{\text{syn}} = 2.7\,\mu S$.

For different activity sequences $a, b, = 1, 2, 3, ...$, that is $A \to B \to C$, $A \to C \to B$, etc, we quantify the differences in the average KC response using the average response for each KC $i = 1, 2, ..., n_{\text{KC}}$ over the time T during which each sequence was presented to the KC. This average response of each KC is $s_i^{(a)} = \frac{n_i^{(a)}}{T}$ where $n_i^{(a)}$ is the number of spikes KC i fired during T. The average intensity of response over all KCs to the presentation of sequence a is given as

$${A_a}^2 = \sum_{i=1}^{n_{\text{KC}}} (s_i^{(a)})^2. \quad (2)$$

The difference in the KC response to two sequences a and b is indicated by

$${\Delta_{ab}}^2 = \sum_{i=1}^{n_{\text{KC}}} (s_i^{(a)} - s_i^{(b)})^2 \quad (3)$$

such that the *relative* difference per response intensity is

$${\delta_{ab}}^2 = \frac{{\Delta_{ab}}^2}{{A_a}^2 + {A_b}^2}. \quad (4)$$

This ratio lies between 0 and 1. In Figure 5 this ratio is shown for some values of the strength and the time scale of the local synapses in the KC lattice.

The total activity grows with increasing strength of the local connections. At $k_{\text{syn}} \approx 2.1\,\mu S$ ($\tau =$

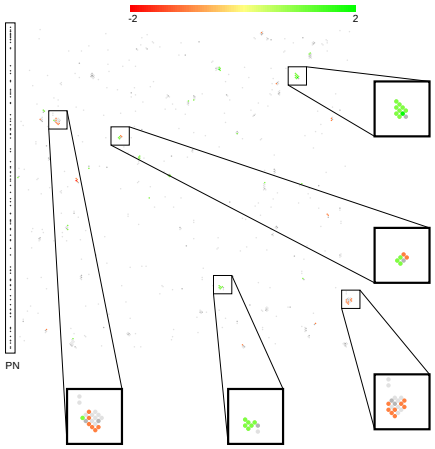

Figure 3: Differences in the average activity of individual PN and KC for local synapses with time constant $\tau_{\text{syn}} = 40\,ms$ and synaptic strength $k_{\text{syn}} = 2.5\,\mu S$. (See the equations for synaptic current in Appendix A.) All PNs and KCs are represented as small dots. The PNs are shown in a single column on the left side. The KCs are arranged on a 2d hexagonal lattice reflecting their axo-axonal neighborhood structure. The average activity of the cells is shown in a greyscale ranging from no activity (white) to maximal activity (total 5 spikes, black). The PN which are much more active than the KC and therefore darker. Superimposed on this image is the difference in activity in a color code. Here the scale ranges from red (2 more spikes in $A \to C \to B$ than in $A \to B \to C$) to green (2 more spikes in $A \to B \to C$ than in $A \to C \to B$). Note that there is no difference in the average activity of the PNs. The *average* activity in the sequence $A \to B \to C$ per KC and per ms is $0.13 \pm 1.3 \cdot 10^{-4}$. The *average* activity of the *active* neurons is $1.2 \pm 0.4 \cdot 10^{-3}$ spikes per ms corresponding to 1.2 spikes in the whole $1000\,ms$ period. The number of active KC is 544. The *average* activity is similar for the other sequences. The boxes at the bottom and right side highlight and magnify regions in the KC lattice that illustrate the results most clearly.

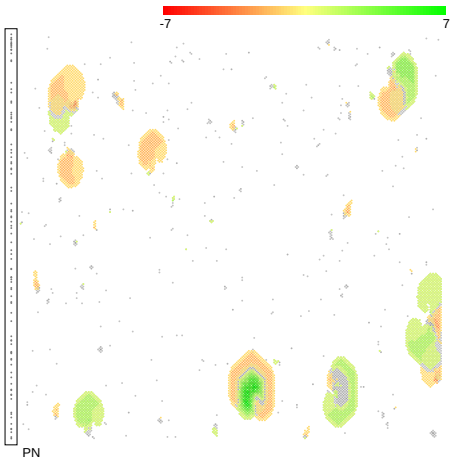

Figure 4: Differences in the average activity of individual PN and KC for local synapses with $\tau_{\text{syn}} = 40\,ms$ and $k_{\text{syn}} = 2.7\,\mu S$. The arrangement is as in figure 3 but the color coding here ranges up to 7 more spikes for one sequence over the other. The greyscale is from 0 spikes to 10 spikes. Even though the time scale and strength of local synapses is clearly below the propagating wave threshold ongoing input from the PN leads to a driven propagation of wavefronts. The specificity to the input is not lost as the shown large differences between the activity for input $A \to B \to C$ and $A \to C \to B$ indicate. The *average* activity per KC and per ms in this case is $1.1 \pm 5.3 \cdot 10^{-4}$. The *average* activity of the *active* neurons is $1.8 \pm 1.3 \cdot 10^{-3}$ spikes per ms corresponding to 1.8 spikes in the whole $1000\,ms$ period. The number of active KC is 3084. The *average* activity is similar for the other sequences. Note that the colored areas consist of individual active neurons. Thus the size of the areas gives a good impression of the total number of KCs involved in the response.

$30\,ms$) and $k_{\text{syn}} \approx 2.6\,\mu S$ ($\tau = 40\,ms$) the critical value for the onset of forced propagating waves is reached resulting in an abrupt change in the slope of the activity curve. Note the logarithmic scale on the y axis in the upper panels in figure 5. The earlier onset of forced propagating waves for faster synapse time scales is explained by the fact that the maximum of the typical EPSP elicited by the local synapses is greater for the faster time scales. If plotted versus the maximum of the EPSP the curves for different time scales more or less coincide, see e.g. figure 5, lower right panel.

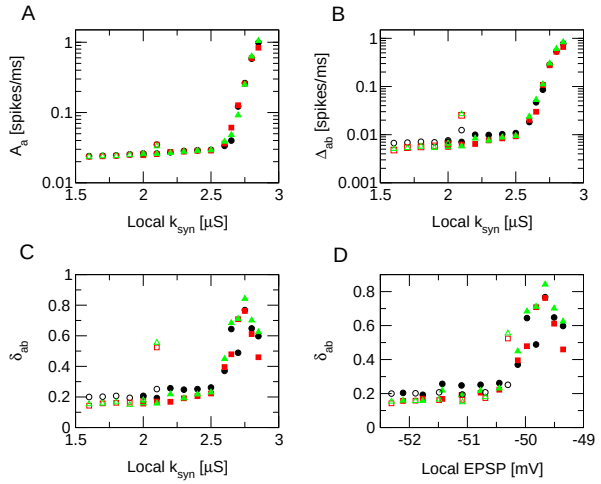

Figure 5: Overview over the dependence of the difference in average activity on the synaptic strength of the local connections. Panel A shows the total average activity. The three symbols correspond to the three tested input sequences. Panel B displays the total distance between the activities corresponding to the three possible combinations of input sequences. Panel C shows the difference normalized by the activity of the sequences versus the strength of local connections and panel D shows the same data versus the size of the maximal membrane potential of a typical EPSP evoked by one of the local synapses. Note that the distances between the activity pattern generated by one of the input sequences and that caused by another sequence are very similar for all the possible combinations. It is also remarkable that when displayed versus the EPSP size the data for different time scales of the local synapses collapse onto the same curve. $\tau_{\text{syn}} = 40\,ms$ (filled symbols) and $30\,ms$ (open symbols).

It is remarkable that the distances between the activities for sequences that differ in the last two groups and those who differ at the beginning are of the same order of magnitude for most of the time even though one would naively expect that the identity of the first group matters most.

There is a local maximum of the relative difference in activities for $k_{\text{syn}} \approx 2.75\,\mu S$ ($\tau = 40\,ms$) suggesting an optimal value for the strength of local connections in the MB. Note, however, that this is already in the regime of forced propagating waves which might conflict with the concept of sparse coding.

6 Discussion

We have demonstrated that under biologically reasonable assumptions the MB of the locust can function as a device to transform a dense spatio-temporal code into a sparse spatial code. In particular it has been shown that slow local excitatory connections allow one to decode the temporal information in the input. Underlying this transformation is a mechanism to decode spatio-temporal neural information that is based on coincidence detection and slow excitation. It does not need any specific connectivity between PNs and KCs.

While using several known properties of the biological system as an input this modeling study also provides clear predictions about the necessary properties of the local connections in the MB. An experimental test for the the mechanism suggested in this study is to measure the EPSPs generated by the local axo-axonal connections among KCs. The EPSPs should outlast the duration of a resetting cycle by the global inhibition of the LHIs. Furthermore, we predict a range for the strength (maximal conductivity) of these connections.

Our interpretation of the sparse spatial code generated in the MB assumes integrators of the KC activity in downstream neural circuitry. The formation of local clusters suggests that it might be advantageous for these integrators to receive input that is local with respect to the axo-axonal KC lattice structure. There are indications from staining experiments in cockroaches which might suggest such a connectivity [Strausfeld and Li, 1999; Strausfeld et al., 2000]. It is, however, an open question on what time scale such downstream integrators might operate. The mechanism suggested here points to a long integration window because otherwise the decoded temporal part of the information might be lost.

One might hope that the formation of small clusters of activity in the KCs of the mushroom body might be detectable in optical or tetrode recordings. The clusters form with respect to the neighborhood structure defined by the axo-axonal connections, however. This neighborhood structure does not correlate well with the spatial arrangement of

the KCs one can see in experiments such that the clusters *cannot* be seen directly.

There are several future directions for this research. One important question is how learning can be included into the current scheme. There are clear indications that the MB is involved in learning and memory of olfactory information [Heisenberg, 2003; de Belle and Heisenberg, 1994; Hammer and Menzel, 1998; Dubnau et al., 2001]. Another project is to move to more and more realistic input from the AL including asynchronous input if no odor is present, noise and eventually input from a realistic AL model.

Acknowledgments

We are grateful to Gilles Laurent for many helpful discussions. This work was partly supported by the U.S. Department of Energy, Office of Basic Energy Sciences, Division of Engineering and Geosciences, under Grants No. DE-FG03-90ER14138 and No. DE-FG03-96ER14592, by grants from the National Science Foundation, NSF PHY0097134 and NSF EIA0130708, by a grant from the Army Research Office, DAAD19-01-1-0026, by a grant from the Office of Naval Research, N00014-00-1-0181, and by a grant from the National Institutes of Health, NIH R01 NS40110-01A2.

A Model components

All synapses in the system were represented by a model first introduced by Rall [Rall, 1967; Rall, 1989] and now is a standard model for synapses [Destexhe et al., 1998]. The synaptic current into a postsynaptic neuron with membrane potential $V_{\rm post}(t)$ is given as

$$I_{\rm Synapse} = -k_{\rm syn}\, g(t)\, (V_{\rm post}(t) - V_{\rm syn}), \qquad (5)$$

where $g(t)$ satisfies

$$\begin{aligned} \frac{df(t)}{dt} &= \frac{1}{\tau_{\rm syn}} \left(\Theta(V_{\rm pre}(t) - V_{\rm th}) - f(t)\right) \\ \frac{dg(t)}{dt} &= \frac{1}{\tau_{\rm syn}} \left(f(t) - g(t)\right), \end{aligned} \qquad (6)$$

$V_{\rm th} = -20\,mV$, and $V_{\rm syn} = 0\,mV$ for excitatory and $V_{\rm syn} = -92\,mV$ for inhibitory synapses. $V_{\rm pre}(t)$ and $V_{\rm post}(t)$ are the pre- and post-synaptic membrane potentials and $\tau_{\rm syn}$ and $k_{\rm syn}$ are the time scale and the strength of the synapse respectively. $\Theta(u) = 0, u \le 0$ and $\Theta(u) = 1, u > 0$ is the usual Heaviside function.

The PNs of the AL were represented by Hodgkin-Huxley type model neurons previously developed for simulations of the AL itself. The equations of these conductance based model neurons are

$$\begin{aligned} C\frac{dV(t)}{dt} = -\big(&I_{\rm Na}(t) + I_{\rm K}(t) + I_{\rm Ca}(t) + I_{\rm KCa}(t) \\ &+ I_l(t)\big) + I_{\rm Synapse}(t), \end{aligned} \qquad (7)$$

where $V(t)$ is the membrane voltage, $C = 1.0\,\mu$F is the membrane capacitance, and the ion currents are determined by

$$\begin{aligned} I_{\rm Na}(t) &= m(t)^3 h(t) g_{\rm Na}(V(t) - V_{\rm Na}) \\ I_{\rm K}(t) &= n(t)^4 (V(t) - V_{\rm K}) \\ I_{\rm Ca}(t) &= k(t)^3 l(t) g_{\rm Ca} \frac{V(t)}{1 - e^{2V(t)/k_{Ca}}} \\ I_{\rm KCa}(t) &= g_{\rm KCa}(V(t) - V_{\rm KCa}) \frac{\omega(t)^4}{k_{\rm KCa}^4 + \omega(t)^4}, \end{aligned} \qquad (8)$$

and the leak current is

$$I_l(t) = g_l(V(t) - V_l). \qquad (9)$$

$I_{\rm Synapse}$ is as given above. We used the following values for the maximal conductances and reversal potentials: $g_l = 0.1\,\mu S$, $g_{\rm Na} = 50\,\mu S$, $g_{\rm K} = 10\,\mu S$, $g_{\rm Ca} = 0.2\,\mu S$, $g_{\rm KCa} = 0.15\,\mu S$, $V_l = -55\,mV$, $V_{\rm Na} = 50\,mV$, $V_{\rm K} = -95\,mV$, $V_{\rm KCa} = -95\,mV$, and the constants are $k_{\rm KCa} = 0.15$ and $k_{\rm Ca} = 24.42\,mV$.

Each of the activation and inactivation functions $m(t)$, $h(t)$, $n(t)$, $k(t)$, and $l(t)$ satisfy first order kinetics equations of the form

$$\frac{dX(t)}{dt} = A_X(V(t)) - B_X(V(t))X(t), \qquad (10)$$

where for $X(t) = m(t), h(t)$, and $n(t)$

$$\begin{aligned}
A_X(V) &= \alpha_X(V) \\
B_X(V) &= \alpha_X(V) + \beta_X(V) \\
\alpha_m(V) &= 0.116\,\frac{V + 42\,mV}{1 - \exp(-(V + 42\,mV)/4\,mV)} \\
\beta_m(V) &= -0.093\,\frac{V + 15\,mV}{1 - \exp((V + 15\,mV)/5\,mV)} \\
\alpha_h(V) &= 0.0426\exp(-(V + 38\,mV)/18\,mV) \\
\beta_h(V) &= \frac{1.33}{1 + \exp(-(V + 15\,mV)/5\,mV)} \\
\alpha_n(V) &= 0.01\,\frac{V + 30\,mV}{1 - \exp(-(V + 30\,mV)/5\,mV)} \\
\beta_n(V) &= 0.166\exp(-(V + 35\,mV)/40\,mV). \quad (11)
\end{aligned}$$

For $k(t)$ and $l(t)$ we have

$$\begin{aligned}
A_X(V) &= \frac{\alpha_X(V)}{\beta_X(V)} \\
B_X(V) &= \frac{1}{\beta_X(V)} \\
\alpha_k(V) &= \frac{1}{1 + \exp(-(V + 27.1\,mV)/7.18\,mV)} \\
\beta_k(V) &= 20 - \frac{19.9}{1 + \exp((V - 40.1)/8\,mV)} \\
\alpha_l(V) &= \frac{1}{1 + \exp((V + 27.0\,mV)/3.5\,mV)} \\
\beta_l(V) &= 30 + \frac{100}{1 + \exp((V + 50.1\,mV)/5\,mV)}.
\end{aligned} \quad (12)$$

The Ca induced K current activation is governed by $\omega(t)$ satisfying

$$\frac{d\omega(t)}{dt} = 0.001\big(-\frac{I_{Ca}(t)}{\mu\mathrm{A}} - c_0^2\,\omega(t) + 0.04\,c_0^2\big), \quad (13)$$

and $c_0 = 1.8$.

The PNs are induced to spike by input received from artificial input neurons which fire rectangular spikes according to the chosen input pattern and are connected to the PNs by Rall type synapses with $\tau_{\mathrm{syn}} = 1.0\,ms$ and $k_{\mathrm{syn}} = 0.8\,\mu S$.

Using such an elaborated neuron model for the PN, which are not the focus of interest in this study, might seem like overkill but will allow to easily combine earlier studies of the AL with the present one in future work. Note that in investigations of the AL appropriate neuron models are important for reproducing the complex spatio-temporal dynamics [Laurent et al., 2001; Rabinovich et al., 2001; Bazhenov et al., 2001b; Bazhenov et al., 2001a].

The KC were represented by leaky integrate and fire neurons (IF) described by

$$C\frac{dV(t)}{dt} = -I_l(t) + I_{\mathrm{Synapse}}(t), \quad (14)$$

where

$$I_l(t) = g_l(V(t) - V_l), \quad (15)$$

$I_{\mathrm{Synapse}}(t)$ is the synaptic input current given above, $g_l = 0.3\,\mu S$ and $V_l = -60\,mV$. If $V(t)$ grows larger than a given threshold $V_{\mathrm{thresh}} = -35\,mV$ it is instantaneously set to the firing voltage $V_{\max} = 50\,mV$. This voltage is fixed for the duration of the firing time $\tau_{\mathrm{f}} = 1.5\,ms$ and then released to develop according to (14). The observed refractoriness of real KC in the MB of the locust was implemented by self-inhibition of these IFs through synapses with $\tau_{\mathrm{syn}} = 45.0\,ms$ and $k_{\mathrm{syn}} = 8\,\mu S$. Using a highly simplified neuron model for the KCs seems to be legitimate because of the simple sparse activity observed in experiments [Perez-Orive et al., 2002]. It allowed us to simulate the system in its full size because of computational simplicity.

The LHIs were represented by a single neuron with slow calcium dynamics only, in particular

$$\frac{dV(t)}{dt} = -\frac{1}{C}(I_l(t) + I_{\mathrm{Ca}}(t) + I_{\mathrm{KCa}}(t) - I_{\mathrm{Synapse}}), \quad (16)$$

where

$$\begin{aligned}
I_l(t) &= g_l(V(t) + 65\,mV) \\
I_{\mathrm{Ca}}(t) &= g_{\mathrm{Ca}}\,k(t)^3\,l(t)\,\frac{V(t)}{1 - \exp(2V(t)/k_{\mathrm{Ca}})} \\
I_{\mathrm{KCa}}(t) &= g_{\mathrm{KCa}}\,\frac{\omega(t)^4}{\omega(t)^4 + 0.5^4}(V(t) + 70\,mV), \quad (17)
\end{aligned}$$

and $g_l = 0.4\,\mu S$, $g_{\mathrm{Ca}} = 2.5\,\mu S$, $g_{\mathrm{KCa}} = 2.0\,\mu S$, and again $k_{\mathrm{Ca}} \approx 24.42\,mV$. This neuron receives input from all PN through excitatory synapses with $\tau_{\mathrm{syn}} = 3.0\,ms$ and $k_{\mathrm{syn}} = 0.023\,\mu S$ and projects to all KC with inhibitory synapses with $\tau_{\mathrm{syn}} = 4.5\,ms$ and $k_{\mathrm{syn}} = 1.0\,\mu S$. We chose this type of neuron

model because the action of the LHI neurons results in a with period $50\,ms$ rather slow periodic inhibition onto the KCs. The slow dynamics of our inhibitory neuron reflects this slower time scale.

B Connectivity analysis

In order to build a realistic model, the parameters of the model neurons and synapses have to be adjusted to a meaningful regime. Calculating the probabilities and expectation values for the number of connections to active neurons as well as the size and form of typical EPSPs in the system allows us to adjust the firing threshold of the model KC and the synaptic strengths of the PN-KC connections to yield a realistic activity in the KC lattice. As the numbers of PNs and KCs are fairly large the law of large numbers is in our favor and the calculation of expectation values provides a very good estimates for the degree of coincidence and the resulting activity in the KC network for a given input.

The EPSP of Rall type synapses onto IF neurons given a square pulse input of duration t_0 is

$$E(t) = \begin{cases} \Big[\int_0^t dt'\, \frac{1}{C} g_l E_l\, e^{\frac{1}{C}(g_l t' + g_{\mathrm{syn}} u(t'))} \\ \quad + E_l\, e^{\frac{2}{C} g_{\mathrm{syn}} \tau_{\mathrm{syn}}} \Big] & t \le t_0 \\ \times\, e^{-\frac{1}{C}(g_l t + g_{\mathrm{syn}} u(t))} \\ \Big[\int_{t_0}^t dt'\, \frac{1}{C} g_l E_l\, e^{\frac{1}{C}(g_l t' + g_{\mathrm{syn}} v(t'))} \\ \quad + E(t_0)\, e^{\frac{1}{C}(g_l t_0 + g_{\mathrm{syn}} v(t_0))} \Big] & t > t_0 \\ \times\, e^{-\frac{1}{C}(g_l t + g_{\mathrm{syn}} v(t))} \end{cases} \tag{18}$$

where

$$u(t) = t(1 + e^{t/\tau_{\mathrm{syn}}}) + 2\tau_{\mathrm{syn}} e^{-t/\tau_{\mathrm{syn}}} \tag{19}$$

$$v(t) = -\big(r(t_0)(\tau_{\mathrm{syn}} + t - t_0) + s(t_0)\tau_{\mathrm{syn}}\big) e^{(t-t_0)/\tau_{\mathrm{syn}}} \tag{20}$$

$$r(t) = 1 - e^{-t/\tau_{\mathrm{syn}}} \tag{21}$$

$$s(t) = s(t) = 1 - (t/\tau_{\mathrm{syn}} + 1) e^{-t/\tau_{\mathrm{syn}}} \tag{22}$$

From this it is easy to obtain the maximal value of the EPSP. Solving for this maximum being equal to the threshold $V_{\mathrm{thresh}} = -35\,mV$ of the IF neurons,

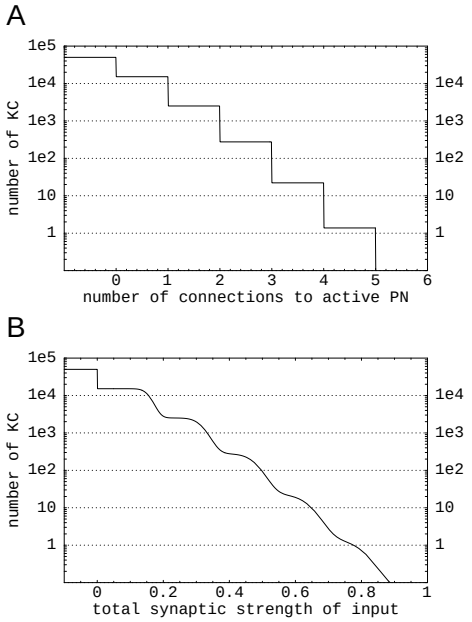

Figure 6: Expectation value for the number of KC with more than x inputs from active PNs (A) and a stronger total input than θ assuming synaptic strengths of PN-KC synapses according to (1) with $\bar{g} = 0.16$ and $\sigma = 0.02$ (B).

one obtains a threshold θ for the total synaptic input strength necessary to fire the neuron. Inserting the parameter values $C = 1\mu F$, $g_l = 0.3\,\mu S$, $E_l = -60\,mV$, $\tau_{\mathrm{syn}} = 1\,ms$, $t_0 = 2.5\,ms$ one obtains $\theta \approx 0.49\,\mu S$.

The random connectivity between AL and KC implemented in the model allows us to calculate the probability distribution for the total synaptic input strengths at the KCs. Let $\mathbf{C} = (c_{ij})$, $i = 1, \ldots, n_{\mathrm{PN}}$, $j = 1, \ldots, n_{\mathrm{KC}}$ denote the connectivity matrix between the PNs and the KCs and let $\mathbf{C}^A = (c^A_{ij})$ denote the connectivity matrix of *active* PNs to all KCs. The probability $P(\sum_i c^A_{ij} = x)$ for a given KC to have x connections to the n_A active PNs is given by the binomial distribution $b_{n_A,p}$ where p is the probability of each individual PN to be connected to a given KC. To have more than θ connections the probability is the sum $p_\theta = \sum_{\lceil\theta\rceil}^{n_A} b_{n_A,p}$. The number N_θ of KCs which have more than θ thus is distributed with a binomial distribution $b_{n_{\mathrm{KC}},p_\theta}$. These considerations give the expectation values for N_θ shown in figure 6A.

Assuming identical synaptic strength for all

synapses, the number of excited KCs given a certain input activity n_A jumps discontinuously as a function of the firing threshold θ. This does not allow a meaningful adjustment of θ to the experimentally observed activity level in the KCs. If one assumes a small jitter in the synaptic strength however, the picture changes dramatically. Let the synaptic strength of the synapses be given by 1. The sum of synaptic strengths of incoming PN input to any KC is then distributed according to

$$\hat{p}_\theta = P(\sum_{i=1}^{n_A} \hat{c}_{ij}^A > \theta) = \sum_{k=0}^{n_A} b_{n_A,p}(k)(1 - \Phi_{\sigma\sqrt{k}}(\theta - kg)) \tag{23}$$

where $\Phi_{\sigma\sqrt{k}}$ denotes the integrated Gaussian distribution with mean 0 and standard deviation $\sigma\sqrt{k}$. And the number $\hat{N}_\theta$ of KCs having stronger input than θ is again a binomial distribution with n_{KC} and $\hat{p}_\theta$. The expectation value for $\hat{N}_\theta$ is shown in figure 6B. The smooth variation of the expectation value of $\hat{N}_\theta$ with varying θ now allows us to adjust θ (or equivalently $\bar{g}$) to a value consistent with the experimentally observed activity levels in the MB.

Aiming for an initial activity of $\approx$ 100 spikes and choosing the jitter of synaptic strengths to be $\sigma = 0.02\,\mu S$ we can calculate the appropriate mean synaptic strength $\bar{g}$ by inverting above equation for the expectation value of $\hat{N}_\theta$ with the $\theta = 0.49$ obtained from the above consideration of the EPSPs. This yields $\bar{g} \approx 0.16$ which has been used consistently in all simulations in this work.

The reasoning for the time constants and strength of the local axo-axonal connections in the KC lattice is along the following lines. The time scale needs to be long enough and the connections need to be strong enough for a significant contribution of local connections to the ongoing activity of the KC ensemble according to the mechanism described in section 3. On the other hand they have to stay below the propagating wave limit to avoid over-excitation of the system.

From the explicit solution for the EPSPs (18) one can estimate the propagating wave threshold assuming a maximum of two simultaneously active neighbors. Choosing $40\,ms$ and $30\,ms$ as example time scales this allows synaptic strengths up to $4.7\,\mu S$ and $3.5\,\mu S$ respectively. These values do not take into account the ongoing input from the AL however. Therefore, *driven* propagating waves already occur for considerably smaller values.

References

Ahissar E, Haidarliu S, Zacksenhouse M [1997] Decoding temporally encoded sensory input by cortical oscillations and thalamic phase comparators. *PNAS* 94: 11633–11638.

Ahissar E, Sosnik R, Haidarliu S [2000] Transformation from temporal to rate coding in a somatosensory thalamocortical pathway. *Nature* 406: 302–306.

Bazhenov M, Stopfer M, Rabinovich MI, Abarbanel HDI, Sejnowski T, Laurent G [2001a] Model of cellular and network mechanisms for odor-evoked temporal patterning in the locust antennal lobe. *Neuron* 30: 569–581.

Bazhenov M, Stopfer M, Rabinovich MI, Huerta R, Abarbanel HDI, Sejnowski T, Laurent G [2001b] Model of transient oscillatory synchronization in the locust antennal lobe. *Neuron* 30: 553–567.

Buonomano DV, Hickmott PW, Merzenich MM [1997] Context-sensitive synaptic plasticity and temporal-to-spatial transformations in hippocampalslices. *PNAS* 94: 10403–10408.

Buonomano DV, Merzenich MM [1995] Temporal information transformed into a spatial code by a neural network with realistic properties. *Science* 267: 1028–30.

de Belle JS, Heisenberg M [1994] Associative odor learning in Drosophila abolished by chemical ablation of mushroom bodies. *Science* 263: 692–695.

Destexhe A, Mainen ZF, Sejnowski TJ [1998] Kinetic models of synaptic transmission In Koch C, Segev I, editors, *Methods in Neuronal Modeling, 2nd Ed.*, pp. 1–26, Cambridge, MA. MIT Press.

Dubnau J, Grady L, Kitamoto T, Tully T [2001] Disruption of neurotransmission in Drosophila mushroom body blocks retrieval but not acquisition of memory. *Nature* 411: 476–480.

Fortin NJ, Agster KL, Eichenbaum HB [2002] Critical role of the hippocampus in memory for sequence of events. *Nature Neurosci.* 5: 458–462.

Hammer M, Menzel R [1998] Multiple sites of associative odor learning as revealed by local brain microinjections of octopamine in honeybees. *Learn. Mem.* 5: 146–156.

Heisenberg M [2003] Mushroom body memoir: From maps to models. *Nat. Rev. Neurosci.* 4: 266–75.

Jeffres LA [1948] A place theory of sound localization. *J. Comp. Physiol. Psychol.* 41: 35–39.

Laurent G [1999] A systems perspective on early olfactory coding. *Science* 286: 723–728.

Laurent G, MacLeod K, Wehr M [1998] Spatiotemporal structure of olfactory inputs to the mushroom bodies. *Learn. & Mem.* 5: 124–132.

Laurent G, Stopfer M, Friedrich RW, Rabinovich MI, Abarbanel HDI [2001] Odor encoding as an active, dynamical process: Experiments, computation, and theory. *Annu. Rev. Neurosci.* 24: 263–297.

Laurent G, Wehr M, Davidowitz H [1996] Temporal representations of odors in an olfactory network. *J. Neurosci.* 16: 3837–3847.

Leibold C, Kempter R, van Hemmen JL [2002] How spiking neurons give rise to a temporal-feature map: From synaptic plasticity to axonal selection. *Phys. Rev. E* 65: 051915.

Leitch B, Laurent G [1996] GABAergic synapses in the antennal lobe and mushroom body of the locust olfactory system. *J. Comp. Neurol.* 372: 487–514.

Lu T, Liang L, Wang X [2001] Temporal and rate representations of time-varying signals in the auditory cortex of awake primates. *Nat. Neurosci.* 4: 1131–1138.

Perez-Orive J, Mazor O, Turner GC, Cassenaer S, Wilson RI, Laurent G [2002] Oscillations and sparsening of odor representations in the mushroom body. *Science* 297: 359–365.

Rabinovich M, Huerta R, Bazhenov M, Kozlov K, Abarbanel HDI [1998] Computer simulations of stimulus dependent state switching in basic circuits of bursting neurons. *Phys. Rev. E* **58**: 6418.

Rabinovich M, Volkovskii A, Lecanda P, Huerta R, Abarbanel HDI, Laurent G [2001] Dynamical encoding by networks of competing neuron groups: Winnerless competition. *Phys. Rev. Lett.* 87: 068102.

Rall W [1967] Distinguishing theoretical synaptic potentials computed for different soma-dendritic distributions of synaptic inputs. *J. Neurophys.* 30: 1138–1168.

Rall W [1989] Cable theory for dendritic neurons In Koch C, Segev I, editors, *Methods in Neuronal Modeling: From synapses to networks*, pp. 9–62, Cambridge. MIT Press.

Reich DS, Mechler F, Purpura KP, Victor JD [2000] Interspike intervals, receptive fields, and information encoding in primary visual cortex. *J. Neurosci.* 20: 1964–1974.

Reich DS, Mechler F, Victor JD [2001] Temporal coding of contrast in primary visual cortex: When, what, and why. *J. Neurophysiol.* 85: 1039–1050.

Reinagel P, Reid RC [2000] Temporal coding of visual information in the thalamus. *J. Neurosci.* 20: 5392–5400.

Stopfer M, Bhagavan S, Smith B, Laurent G [1997] Impaired odor discrimination on desynchronization of odor-encoding neural assemblies. *Nature* 390: 70–74.

Stopfer M, Jayaraman V, Laurent G [2003] Spatiotemporal code for odor identity and concentration. *in preparation* .

Strausfeld NJ, Homberg U, Kloppenburg P [2000] Parallel organization in honey bee mushroom bodies by peptidergic Kenyon cells. *J. Comp. Neurol.* 428: 760.

Strausfeld NJ, Li Y [1999] Representation of the calyces in the medial and vertical lobes of cockroach mushroom bodies. *J. Comp. Neurol.* 409: 626–46.

Teyke T, Gelperin A [1999] Olfactory oscillations augment odor discrimination not odor identification by Limax CNS. *Neuro Report* 10: 1061–1068.

v. Rullen R, Thorpe SJ [2001] Rate coding versus temporal order coding: What the retinal ganglion cells tell the visual cortex. *Neural Comp.* 13: 1255–1283.

Wallenstein GV, Eichenbaum H, Hasselmo ME [1998] The hippocampus as an associator of discontiguous events. *Trends Neurosci.* 21: 317–323.

Wehr M, Laurent G [1996] Odor encoding by temporal sequences of firing in oscillating neural assemblies. *Nature* 384: 162–166.

Wehr M, Laurent G [1999] Relationship between afferent and central temporal patterns in the locust olfactory system. *J. Neurosci.* 19: 381–390.